

north, on 27 March, shows a focal mechanism similar to that of the main shock (Fig. 4 bottom). This suggests that the main-shock rupture may have propagated beyond the limits of the background seismicity in this region, or at least triggered aftershocks within the normally aseismic region surrounding the seismically active slab.

Recent research suggests that deep earthquakes may be caused by transformational faulting, as material within a wedge of metastable olivine^{21,23} is transformed to a spinel structure^{5,6,24,25}. Because the transformation is temperature-activated, deep earthquakes should occur preferentially in the warmer, outer regions of the metastable wedge, possibly forming a double seismic zone^{15,26}. The background seismicity near the 9 March event, when viewed in cross-section, shows two rather indistinct vertical alignments of earthquakes along the edges of the slab that may represent such a double seismic zone (blue ellipses in Fig. 3c).

The zone of aftershocks of the 9 March event cuts across the entire zone of seismicity and some distance into the surrounding aseismic region, extending for at least 55 km in a direction perpendicular to slab strike. Although it may be possible that the main-shock rupture did not extend all the way to the outer aftershocks, the two aftershocks unmistakably initiated outside the normal zone of seismicity. The 55 km width of the aftershock zone exceeds both the width of the background seismicity in the slab (Fig. 3c) and current estimates of the width of the metastable wedge^{15,27} based on slab thermal models²⁸ and the kinetics of the olivine–spinel reaction^{21,23} (~20 km at this depth in the Tonga slab). We propose that either the metastable olivine wedge is much wider than previously thought, because of deficiencies in the thermal models or kinetic calculations, or that the aftershocks are not confined within such a wedge. The first option seems unlikely, as it requires an explanation for the confinement of the background seismicity to a zone much narrower than the metastable wedge. If the aftershocks are occurring outside the zone of metastable olivine, then a mechanism for their occurrence other than transformational faulting must be sought. □

Received 29 August; accepted 15 November 1994.

1. Leith, A. & Sharpe, J. A. *J. Geol.* **44**, 877–917 (1936).
2. Frohlich, C. A. *Rev. Earth planet. Sci.* **17**, 227–254 (1989).
3. Pavlits, G. L. & Hamburger, M. W. *J. geophys. Res.* **96**, 18107–18117 (1991).
4. Kisslinger, C. & Hasegawa, A. *Tectonophysics* **197**, 27–40 (1991).
5. Green, H. W. & Burnley, P. C. *Nature* **341**, 733–737 (1989).
6. Kirby, S. H., Durham, W. B. & Stern, L. A. *Science* **252**, 216–225 (1991).
7. Willemann, R. J. & Frohlich, C. J. *geophys. Res.* **92**, 13927–13943 (1987).
8. Myers, S. C. et al. *Geophys. Res. Lett.* (in the press).
9. Omori, F. *J. Coll. Sci. Imp. Univ. Tokyo* **7**, 111–200 (1895).
10. Kisslinger, C. & Jones, L. M. *J. geophys. Res.* **96**, 11947–11958 (1991).
11. Davis, S. D. & Frohlich, C. J. *Geophys. Res.* **96**, 6335–6350 (1991).
12. Utsu, T. *Geophys. Mag.* **30**, 521–605 (1961).
13. Ogata, Y. *J. Phys. Earth* **31**, 115–124 (1983).
14. Jordan, T. H. & Sverdrup, K. A. *Bull. seism. Soc. Am.* **71**, 1105–1130 (1981).
15. Wiens, D. A., McGuire, J. J. & Shore, P. J. *Nature* **364**, 790–793 (1993).
16. Fuchs, K. & Müller, G. *Geophys. J. R. astr. Soc.* **23**, 417–433 (1971).
17. Kennett, B. L. N. *Seismic Wave Propagation in Stratified Media* (Cambridge Univ. Press, 1983).
18. McGuire, J. J. et al. (abstr.) *EOS* **75**, 466 (1994).
19. Wyss, M. & Molnar, P. *Phys. Earth planet. Inter.* **6**, 279–292 (1972).
20. Houston, H. & Williams, Q. *Nature* **352**, 520–522 (1991).
21. Sung, C. & Burns, R. G. *Tectonophysics* **31**, 1–32 (1976).
22. Idaka, T. & Suetsubo, D. *Nature* **356**, 593–595 (1992).
23. Rubie, D. C. & Ross, C. R. *Phys. Earth planet. Inter.* (in the press).
24. Kirby, S. H. *J. geophys. Res.* **92**, 13789–13800 (1987).
25. Green, H. W., Young, T. E., Walker, D. & Scholz, C. H. *Nature* **348**, 720–722 (1990).
26. Idaka, T. & Furukawa, Y. *Science* **263**, 1116–1118 (1994).
27. Stein, S., Kirby, S. H., Rubie, D. & Okai, E. A. paper presented at the SUBCON conference, Avion, California, 13–17 June 1994.
28. Toksoz, M. N., Sleep, N. H. & Smith, A. T. *Geophys. J. R. astr. Soc.* **35**, 285–310 (1973).
29. Abe, K. *J. Phys. Earth* **30**, 321–330 (1982).
30. Dziewonski, A. M., Chou, T. & Woodhouse, J. H. *J. geophys. Res.* **86**, 2825–2852 (1981).

ACKNOWLEDGEMENTS. Equipment for this research was obtained from the PASSCAL programme of the Incorporated Research Institutes in Seismology. We thank G. Hade and P. Friberg for assistance in deploying the seismographs. We also thank R. van der Hilst for providing data from seismic stations in the Australian SKIPPY deployment, D. Rouland and R. Pillet for providing data from stations in Vanuatu and New Caledonia, T. Wallace for a copy of his paper before publication, and B. Park-Li and R. Sakata for picking phase arrival times. The manuscript was improved by reviews from J. Vidale and H. Green. This work was supported by the US NSF.

Combined spatial and temporal imaging of brain activity during visual selective attention in humans

H. J. Heinze*,†, G. R. Mangun†‡, W. Burchert§,
H. Hinrichs*, M. Scholz*, T. F. Münte||, A. Göss§,
M. Scherg†, S. Johannes||, H. Hundeshagen§,
M. S. Gazzaniga† & S. A. Hillyard#

* Department of Clinical Neurophysiology, Otto-v-Guericke University, D-39120 Magdeburg, Germany

† Department of Psychology and Center for Neuroscience, University of California at Davis, Davis, California 95616, USA

‡ Department of Nuclear Medicine, Medical School of Hannover, 3000 Hannover, Germany

|| Department of Neurology, Medical School of Hannover, 3000 Hannover, Germany

Department of Neurology, University of Heidelberg, Heidelberg, Germany

Department of Neurosciences, University of California at San Diego, La Jolla, California 92093, USA

VISUAL-SPATIAL attention is an essential brain function that enables us to select and preferentially process high priority information in the visual fields^{1,2}. Several brain areas have been shown to participate in the control of spatial attention in humans^{3–5}, but little is known about the underlying selection mechanisms. Non-invasive scalp recordings of event-related potentials (e.r.ps) in humans have shown that attended visual stimuli are preferentially selected as early as 80–90 ms after stimulus onset^{6,7}, but current e.r.p. methods do not permit a precise localization of the participating cortical areas. In this study we combined neuroimaging (positron emission tomography) with e.r.p. recording in order to describe both the cortical anatomy and time course of attentional selection processes. Together these methods showed that visual inputs from attended locations receive enhanced processing in the extrastriate cortex (fusiform gyrus) at 80–130 ms after stimulus onset. These findings reinforce early selection models of attention^{8–10}.

In our spatial attention task, healthy young subjects ($N=10$) attended selectively to the right or left half of bilateral stimulus arrays that were flashed in rapid sequence (Fig. 1, top). Attention was directed covertly while the subjects' gaze remained fixated on a central dot; fixation was verified with both electro-oculographic and high-resolution infrared video methods. Changes in regional cerebral blood flow (activation) as a function of selective attention were measured using the positron emission tomography (PET) $H_2^{15}O$ method. These activations were first visualized as difference images derived by subtracting the images obtained during passive viewing from those obtained in the attend-left or the attend-right conditions (Fig. 1). Focused attention produced significant PET activation in the hemisphere contralateral to the attended visual hemifield (Table 1). Specifically, attending to the left produced a significant activation in the right posterior fusiform gyrus of extrastriate visual cortex (Fig. 1, left column), whereas attending to the right produced activation in the left fusiform gyrus (Fig. 1, right column).

Significant activations were also obtained in the right anterior cingulate gyrus, and left superior frontal gyrus for the attend-left minus passive PET images (Table 1). Significant activations in the thalamus reached statistical significance only for the attend-right minus passive subtraction (Fig. 1). No significant attention-related activations were obtained in the striate cortex or parietal cortex in this task.

† To whom correspondence should be addressed.

TABLE 1 Significant changes in regional cerebral blood flow (activation) as indicated by PET

Types of difference image	Talairach coordinates (mm)			Brain structure	Significance level (<i>P</i>)
	M/L	A/P	S/I		
L-P	10	-1	58	Superior frontal gyrus, left	0.02
	-3	14	34	Cingulate gyrus, anterior right	0.02
	-28	-73	-14	Fusiform gyrus, right	0.02
R-P	1	-18	0	Thalamus	0.01
	27	-77	-14	Fusiform gyrus, left	0.01

The results of two types of subtraction images were investigated using the procedure in ref. 27 (attend-left minus passive = L-P; attend-right minus passive = R-P). For each, the three-dimensional locations of the centre of the activated brain regions is indicated in coordinates of the Talairach and Tournoux atlas²⁸. M/L, Medial-lateral; A/P, Anterior-posterior; S/I, Superior-inferior. The magnitude of the activations varied from 4–6 per cent. The sample variance of the difference images estimated over all subjects was roughly constant over the whole volume, thus allowing the *t*-statistics to be calculated with a fixed standard deviation independent of localization²⁷. A three-dimensional Hanning filter (FWHM = 18.8 mm) was applied to overcome residual anatomical variability. The resulting reduction in spatial resolution is accounted for in the procedure. Weak activations that were not statistically significant were noted for the attend-left minus passive subtraction in the thalamus (*P* = 0.61), and in the region of the left and right insula and claustrum (*P* = 0.48 and *P* = 0.53, respectively). Nonsignificant activations noted in the attend-right minus passive subtraction were in the anterior cingulate gyrus (*P* = 0.34) and in the regions of the right insula and claustrum (*P* = 0.16). Only increases in regional blood flow are described above and in the table: significant decreases in blood flow were observed in inferior-medial regions of the prefrontal cortex in the medial frontal gyrus and the gyrus rectus (Brodmann's areas 10 and 11) for both attend-left minus passive and attend-right minus passive subtractions (both *P* < 0.01).

The e.r.ps were recorded in a separate session from the same subjects performing the identical spatial attention task. The early positive P1 component (80–130 ms after stimulus onset) was of significantly greater amplitude over the occipital scalp regions contralateral to the attended hemifield (Fig. 2a), replicating previous reports¹¹. Isovoltage contour maps showed the P1 attention effect to be maximal over the lateral occipital cortex (Fig. 2a). There were no significant attention-related changes in the e.r.p. waveform during the earlier time period from 50–80 ms latency that reportedly corresponds to activity in the primary visual (striate) cortex (*P* > 0.5)^{7,12}.

To rule out the possibility that these attention-related PET activations or e.r.p. differences were the result of nonspecific changes in brain activity between conditions of directed attention versus passive viewing, a second type of difference image was calculated by subtracting the attend-right from the attend-left condition. Such a subtraction compares two selective attention conditions in which the overall level of behavioural arousal was equivalent. In this subtraction, only the PET activations in the fusiform gyrus remained statistically significant. Similarly, the attend-left minus attend-right subtraction for the e.r.ps showed significant (*P* < 0.01) effects of spatial attention in the 80–130 ms time period, with a maximum amplitude over the lateral occipital cortex (Fig. 2b, right).

To examine whether the attention-related neural activity in the fusiform gyrus shown by PET could have produced the recorded e.r.p. voltage patterns on the scalp, we modelled the neural generators of the e.r.p. activity as discrete dipolar sources¹³. To model the attend-left minus right e.r.p. attention effect (Fig. 2b, right), a dipole was placed in each hemisphere at the centre of the fusiform gyrus PET activation, and the dipole orientations were allowed to change to minimize the difference between scalp fields predicted by the forward solution and the recorded e.r.ps.

FIG. 1 Brain regions activated during spatial selective attention. The stimulus array is depicted at top, with the direction of covert attention indicated by the 'spotlight' in broken lines. Subtracted PET images (right hemisphere on right side) for attend-left minus passive (left column) and attend-right minus passive (right column) conditions are overlaid onto the corresponding section from the Talairach Atlas²⁸. Significant activations as a function of spatial attention were localized to the fusiform gyrus in the hemisphere contralateral to the attended visual hemifield (top row images), in the thalamus (second row), and in the anterior cingulate gyrus (bottom row). Scale is per cent maximal activation. Subjects attended to either the left or right half of the flashed (100 ms duration) bilateral stimulus arrays for two blocks each and passively viewed the stimuli for two blocks. The task was to press a button when the two symbols in the attended half-field were identical; these 'targets' occurred on 25% of the trials. Stimulus-onset-asynchronies varied from 250–550 ms. Symbols (each 1.9 × 1.4 degrees) were located 6.0 and 11.0 degrees eccentric (to centre). Mean target detection accuracy was 57.3%, and mean reaction time was 548 ms with false alarms below 10%. Sixty seconds before injection the subjects fixated and the stimuli began. Twenty seconds before injection the subjects were instructed to begin attending and performing the task. A bolus injection of 10 ml saline with 50 mCi of ¹⁵O-labelled water (half-life 123 s) was injected via intravenous catheter in the right arm. Using a SIEMENS ECAT 951/31 scanner, data was acquired 20–60 s after injection. Head position was monitored using ⁶⁸Ge scalp markers. The anterior commissure/posterior commissure line was identified in the subjects' PET-images²⁹ and verified with MRI scans. The PET scans were reoriented and then rescaled into stereotactic space²⁸ and global normalization was performed^{25,30}. The two scans per attention condition were averaged together for each subject and filtered. Difference images were calculated and then averaged over the 10 subjects. Because tissue radiation counts are roughly linear with cerebral blood flow³⁰ the effects were considered to reflect cerebral blood flow. PET activity was also measured in each subject in spherical regions of interest (18.8 mm diameter) centred on the coordinates of maximal significant activations²⁷ for analysis with repeated-measures ANOVA. A significant interaction (*F*[1, 9] = 41.5, *P* < 0.001) of direction of attention (left versus right) and hemisphere of activation (left versus right) indicated that attention produced a contralateral fusiform gyrus activation.

FIG. 3 Correspondence between best-fit dipole of the P1 attention effect and locus of PET activation. Top, Graph represents the 'goodness-of-fit' between the dipole model and observed e.r.p. scalp distribution of attend-left minus attend-right difference waveform at different latencies (50–230 ms), plotted as scalp voltage variance not accounted for (that is, residual variance (RV)) by the seeded (upper trace) or best-fit inverse (lower trace) dipole models. For the seeded dipoles the location was fixed in the fusiform gyrus, but dipole orientations were permitted to vary. Fitting was done over 20-ms windows centred on the time points indicated. In the case of the best-fit inverse solutions, for each time epoch we fit a separate unconstrained best inverse solution for the dipole pair with starting positions in the fusiform gyrus. Lower values of residual variance indicate a close correspondence between the recorded e.r.p. attention effects and the model data. The seeded dipoles accounted for 96.2% of variance in the 110–130 ms interval. The best-fit dipole locations (red circles) were shifted slightly from the centre of the PET activation, but were still in the region of PET activation (black circle); these dipoles explained 98.4% of variance in the 110–130 ms interval. The interval of the best fit corresponded to the peak of the P1 attention effect. Outside this time period the residual variance rose substantially, and the loci of the best-fit inverse solutions (green circles) were variable in their distance from the fusiform gyrus activations. However, in the time range of the P1 attention effect the best-fit inverse dipoles converged on the locus of PET activation, as shown for right hemisphere dipole locations on a Talairach section²⁸ through the fusiform gyrus (bottom).

These 'seeded' dipoles provided a good account of the e.r.p. attention difference maps in the latency range of the P1 attention effect (compare Fig. 2b right, with Fig. 2c right). When the fixed-location constraint on the bilateral dipoles was released to permit the modelling algorithm to obtain the smallest residual difference between model and recorded e.r.p. data, a similarly close correspondence with the observed e.r.p. attention effects was obtained

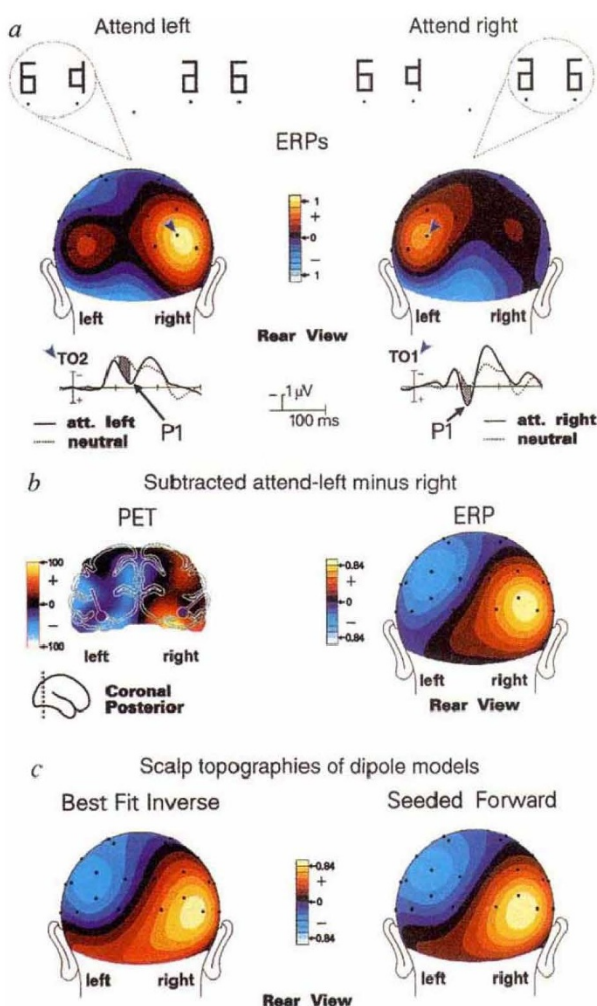
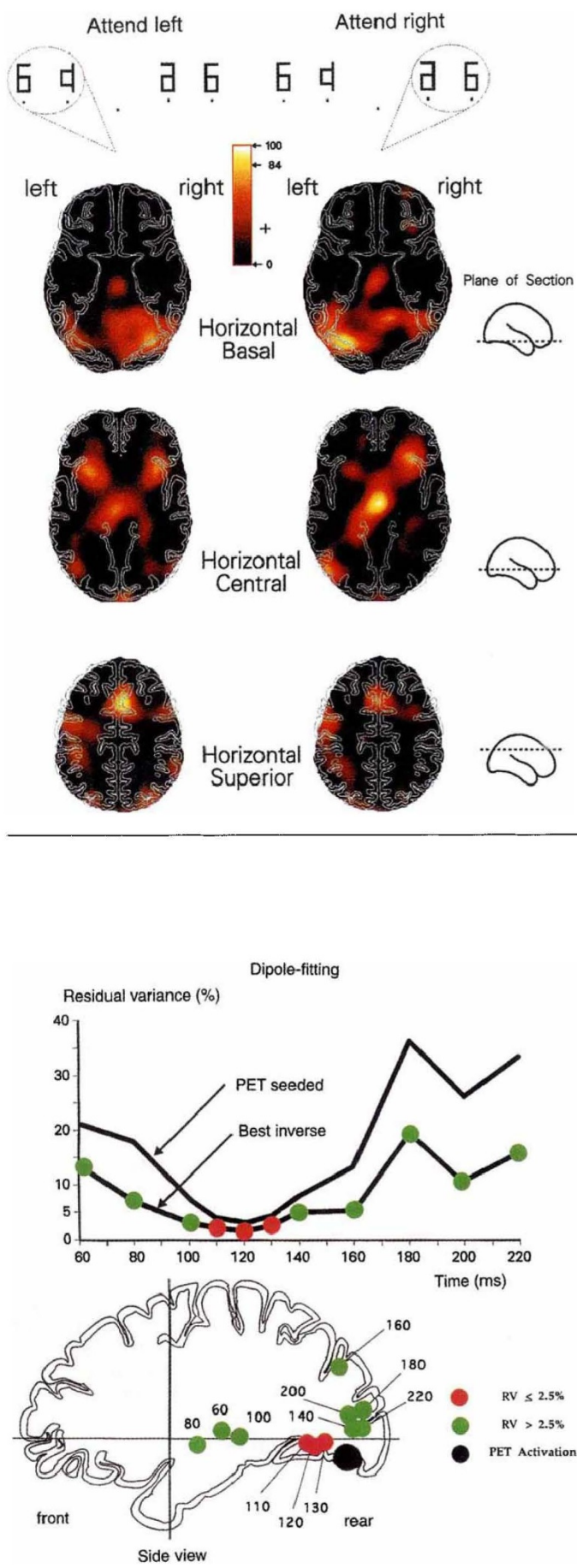


FIG. 2 Comparison of PET and e.r.p. attention effects. The stimuli and tasks were the same in separate PET and e.r.p. sessions, but in the e.r.p. session the subjects received 10 runs in each condition. *a*, Topographic isovoltage contour maps of the P1 attention effect for attend-left minus passive (left column) and attend-right minus passive (right column) conditions; scale is in microvolts. Below each topographic map are the corresponding e.r.p. waveforms and attention effects (ANOVA, 80–110 and 110–130 ms windows, both $P < 0.01$ for direction of attention by hemisphere interaction) recorded from contralateral occipital scalp sites indicated by the arrows (T01 and T02 are halfway from O1 to T5, and O2 to T6 of the International 10–20 System, respectively); shading indicates time period of the maps. *b*, At left is a coronal section through the posterior occipital region showing the attention-specific PET activation in the fusiform gyrus in the attend-left minus attend-right difference image. The fusiform gyrus activations in these subtraction images were significant for both the right fusiform gyrus activation ($t = 4.3$, $P < 0.001$) and the left fusiform gyrus activation ($t = -2.6$, $P < 0.02$); note that the left fusiform gyrus activation is seen as a relative decrease in the figure because of the direction of the subtraction. The dots represent the locations of the best inverse dipole solutions, with dipole orientations indicated by the attached lines. The corresponding attend-left minus attend-right topographic maps for the P1 attention effect are shown at right. *c*, At right, the topographic map derived from model dipolar sources seeded in the centre of the PET activation in fusiform gyrus over the 80–130 ms time range provided a close fit to the recorded P1 attention effect (*b*, right column). The constraint-free best-fit dipoles moved slightly anteriorly and laterally, and the topographic maps showed only minor alterations (left column). For detailed e.r.p. methodology, see ref. 11.

(compare Fig. 2b right, with Fig. 2c left). Thus, the localization of the model dipoles in the region of the PET activation in the posterior fusiform gyrus (Fig. 3) produced a model scalp field with a topography that was highly similar to that of the early P1 attention effect that was actually recorded.

The results from these combined PET and e.r.p. recordings converge in several key respects. First, in line with previous e.r.p. studies in humans^{7,14}, neither the e.r.p. nor PET measurements provided any evidence that spatial attention influences processing in the striate cortex or in the afferent geniculostriate pathways. Second, PET and e.r.p. recordings both showed that neural activity was selectively modulated in the ventral extrastriate visual cortex contralateral to the direction of attention, and that this modulation could be dissociated from nonspecific factors such as arousal or alertness. Finally, dipolar neural generators at the locus of the PET activity in the fusiform gyrus provided a good account of the early ERP attention effect at the scalp between 80–130 ms latency, suggesting that these PET and e.r.p. effects arose from a common source of neural activity.

The finding of attentional modulations in the fusiform gyrus at 80–130 ms latency indicates that spatial attention influences activity in the human occipito-temporal or 'ventral stream' of visual cortical processing to permit inputs from attended regions to gain preferential access to higher stages of feature analysis, pattern identification and object recognition^{15–17}. Similar attentional modulations of neural activity in ventral stream cortical areas have been observed in neurophysiological studies of non-human primates^{18–21}. These attentional mechanisms appear to be controlled by a network of brain structures that includes the posterior parietal lobe, anterior cingulate cortex, and the pulvinar nucleus of the thalamus^{3,5,22–26}. In a previous study that involved the repetitive shifting of attention between locations, activation of the parietal lobes was a prominent finding using PET²⁵. Presumably, such parietal activation was absent in our study because attention was sustained on a given location for several minutes rather than continually shifted between locations. Thus, it appears that sustained focal attention to location engages stimulus selection processes in the ventral extrastriate cortex with minimal activation of the parietal lobes.

Together, these PET and e.r.p. data provide a high-resolution view in both temporal and spatial domains of the earliest changes in visual processing that accompany visual-spatial selective attention in humans. The convergent use of different neuroimaging methods such as PET and e.r.p. recording promises to be a powerful approach for defining the spatial-temporal properties of brain activity underlying cognitive processes such as selective attention. □

Received 2 June; accepted 27 October 1994.

- Hawkins, H. L. et al. *J. exp. Psychol. Hum. Percept. Perform.* **16**, 802–811 (1990).
- Van der Heijden, A. *Selective Attention in Vision* (Routledge, London, 1992).
- Posner, M. I. & Petersen, S. E. *A. Rev. Neurosci.* **13**, 25–42 (1990).
- Posner, M. I. & Driver, J. *Curr. Opin. Neurobiol.* **2**, 165–169 (1992).
- LaBerge, D. *J. cogn. Neurosci.* **2**, 358–372 (1990).
- Hillyard, S. A. *Curr. Opin. Neurobiol.* **3**, 217–224 (1993).
- Mangun, G. R., Hillyard, S. A. & Luck, S. J. in *Attention and Performance XIV* (eds Meyer, D. & Kornblum, S.) 220–243 (MIT Press, Cambridge, MA, 1993).
- Broadbent, D. A. *Perception and Communication* (Pergamon, New York, 1958).
- Posner, M. I., Snyder, C. R. R. & Davidson, B. J. *J. exp. Psychol. Gen.* **109**, 160–174 (1980).
- Treisman, A. *Quart. J. exp. Psychol.* **40**, 201–237 (1988).
- Heinze, H. J. et al. *Percept. Psychophys.* **56**, 42–52 (1994).
- Jeffreys, D. A. & Axford, J. G. *Expl Brain Res.* **16**, 1–21 (1972).
- Scherg, M. & Berg, P. *Brain Topogr.* **4**, 143–150 (1991).
- Gomez Gonzalez, C. M., Clark, V. P., Fan, S., Luck, S. J. & Hillyard, S. A. *Brain Topogr.* (in the press).
- Ungerleider, L. G. & Mishkin, M. in *Analysis of Visual Behavior* (eds Ingle, D. J., Goodale, M. A. & Mansfield, R. J. W.) 549–586 (MIT Press, Cambridge, MA, 1982).
- Tanaka, K., Sugita, Y., Moriya, M. & Saito, H. *J. Neurophysiol.* **69**, 128–142 (1993).
- Zeki, S. et al. *J. Neurosci.* **11**, 641–649 (1991).
- Fischer, B. & Boch, R. *Brain Res.* **345**, 111–123 (1985).
- Moran, J. & Desimone, R. *Science* **229**, 782–784 (1985).
- Spitzer, H., Desimone, R. & Moran, J. *Science* **240**, 338–340 (1988).
- Moeller, B. C. *J. Neurophysiol.* **70**, 909–919 (1993).
- Petersen, S. E., Fiez, J. A. & Corbetta, M. *Curr. Opin. Neurobiol.* **2**, 217–222 (1992).
- Corbetta, M., Miezin, F. M., Dobmeyer, S., Shulman, G. L. & Petersen, S. E. *J. Neurosci.* **11**, 2383–2402 (1991).

- Petersen, S. E., Corbetta, M., Miezin, F. M., Shulman, G. L. & Raichle, M. E. in *Brain Mechanisms of Perception and Memory: From Neuron to Behavior* (eds Ono, T., Squire, L., Perrett, D. & Raichle, M. E.) 413–425 (Oxford Univ. Press, New York, 1993).
- Corbetta, M., Miezin, F. M., Shulman, G. L. & Petersen, S. E. *J. Neurosci.* **13**, 1202–1226 (1993).
- Desimone, R., Wessinger, M., Thomas, L. & Schneider, W. in *Cold Spring Harb. Symp. quart. Biol.* 963–971 (1992).
- Worsley, K. J., Evans, A. C., Marret, S. & Neelin, P. *J. Cereb. Blood Flow Metab.* **12**, 900–918 (1992).
- Talairach, J. & Tournoux, P. *Co-planar Stereotactic Atlas of the Human Brain* 2nd edn (Thieme, Stuttgart, 1988).
- Friston, K. J. et al. *J. Cereb. Blood Flow Metab.* **9**, 690–695 (1989).
- Fox, P. T. & Mintun, M. A. *J. nucl. Med.* **30**, 141–149 (1989).

ACKNOWLEDGEMENTS. We thank M. Woldorff, J. Hansen, M. E. Raichle and S. E. Petersen for their comments and assistance. This work was supported by grants from the Human Frontiers Science Program Organization, the NIMH and NIH, the Deutsche Forschungsgemeinschaft, the ONR and the James S. McDonnell Foundation.

Nitric oxide in skeletal muscle

Lester Kobzik*, Michael B. Reid†, David S. Bredt‡ & Jonathan S. Stamler§||

* Department of Pathology, Brigham and Women's Hospital and Physiology Program, Harvard School of Public Health, Boston, Massachusetts 02115, USA

† Pulmonary and Critical Care Medicine, Baylor College of Medicine, Houston, Texas 77030, USA

‡ Department of Physiology, UCSF, San Francisco, California 94143, USA

§ Department of Medicine, Pulmonary and Cardiovascular Divisions, and Department of Cell Biology, Duke University Medical Center, Box 3177, Durham, North-Carolina 27710, USA

REACTIVE oxygen intermediates modulate skeletal muscle contraction^{1,2}, but little is known about the role of nitric oxide (NO). Here we show that rat skeletal muscle expresses neuronal-type NO synthase and that activity varies among several respiratory and limb muscles. Immunohistochemistry showed prominent staining of type II (fast) fibre cell membranes with antibodies against neuronal-type NO synthase. NO synthase activity in muscles correlated with type II fibre density. Resting diaphragm muscle produced detectable NO_x, but no reactive oxygen intermediates. In contrast, actively contracting muscle generated increased levels of reactive oxygen intermediates. Contractile function was augmented by blockers of NO synthase, extracellular NO chelation, and guanylyl cyclase inhibition; it was depressed by NO donors and by increased levels of cyclic GMP. Force-frequency plots of different muscles showed an inverse correlation between NO synthase activity and force development. Our results support two physiological functions of NO in skeletal muscle. The first is to promote relaxation through the cGMP pathway^{3,4}. The second is to modulate increases in contraction that are dependent on reactive oxygen intermediates and which are thought to occur through reactions with regulatory thiols on the sarcoplasmic reticulum^{5,6}.

During analysis of neuronal-type NO synthase (nc-NOS) localization in rat trachea⁷, we observed prominent immunostaining of adjacent oesophageal skeletal muscle. Encouraged by the observation that nc-NOS messenger RNA is expressed in human skeletal muscle samples⁸, we investigated the production, source and function of NO in mammalian (rat) skeletal muscle.

Biochemical assays of skeletal muscle homogenates showed NO synthase activity (Table 1) was associated with the membrane fraction. Western staining with anti-nc-NOS identified an immunoreactive band of the predicted relative molecular mass (M_r 160 K, not shown) which comigrated with NO synthase from rat cerebellum.

The NO synthase activity of individual muscles correlated strongly with type II fibre composition^{9,10} (Table 1). Immunolocalization showed that nc-NOS antigens were prominent in

|| To whom correspondence should be addressed.